Photometry of the Young Stellar Cluster NGC7160
–
Reaching the Brown Dwarf Limit

Rurik Wahlin, Silva Järvinen, Eva Karlsson, Mathias Egholm

Supervisor: Michael Andersen

September 25, 2003

Contents

1 Introduction

1.1 Brown dwarfs

Brown dwarfs (BD) are objects intermediate between stars and giant planets. The division line between stars and BD's are set at the minimum mass for hydrogen burning at $\sim 0.08 M_{\odot}$. This limit is dependent on metallicity with slightly larger masses at lower metallicity. It is a bit more difficult to discriminate between giant planets and BD's. One suggestion is to set the division line at the lower mass limit for deuterium burning at $\sim 0.01 M_{\odot}$.

BD's were earlier considered as a candidate to the baryonic dark matter. Although they may be about as common as stars they are no longer believed to contribute substantially to the dark matter. One of the primary interests in the observations of BD's is the determination of the low mass initial mass function (IMF). The IMF in turn is needed for instance in the study of the chemical evolution in galaxies and in models of star formation in general.

It is in the nature of the BD's that they will never be stabilized on the main sequence. With the exception of the most massive BD's, who will experience a brief increase in luminosity at early stages, they will become fainter and cooler throughout their life. Because of this they are most easily detected as infants. Open clusters are young stellar systems and therefore we can expect to find a large amount of relatively bright BD's there. By choosing to study BD's in open clusters we can also transfer information gathered from the cluster as a whole or from other cluster members to the BD's. For instance the distance, metallicity, mass and age would be very difficult or impossible to determine from an isolated BD. But for BD's detected in an open cluster these quantities can easily be determined. By analyzing the stellar and substellar content of an open cluster we can also get an idea about the mass function of the cluster. This can then, with a few assumptions, be translated to an IMF.

The first step in the study of a brown dwarf is naturally detection through photometry. Since BD's are so cold they emit most of their radiation in the IR. It would be much more expensive in terms of observation time to get a color magnitude diagram (CMD) in visual filters than in near infrared (NIR) filters.

It is difficult to determine from photometry alone whether a source is a cluster BD or a foreground/background object with similar colors and apparent magnitude. Fortunately there are several ways to distinguish the cluster members from non-cluster members. Among these are determination of proper motion, radial velocities, presence of Hα emission or presence of lithium at masses below the lithium depletion limit.

For reviews of BD's see Chabrier & Baraffe, (2000) and Basri (2000) and references therein.

1.2 Previous observations.

Two fields, covering 5' x 7', in the open cluster NGC 7160 were observed in 1992 by our supervisor, Michael Andersen, in V, I and Hα. The present observations cover the same two fields and these observations can then be used to determine proper motions of the detected objects. The Hα observations together with the proper motions will help to discriminate between cluster members and non cluster members.

The cluster were observed in 1999 by the 2MASS survey in J, H and Ks. Although the upper main sequence is clearly visible in the 2MASS data this survey is not deep enough to detect the cluster BD's or low mass stars. Williams, (1995) studied the cluster in V, I and K band photometry down to masses of $\sim 0.15 M_{\odot}$ and determined the mass function of the cluster. According to a recent proper motion survey of open clusters (Kharchenko, Pakulyak & Piskunov, 2003) the cluster have proper motion equal to μ_α=-2.82, μ_δ=-2.35 mas/yr, the distance to the cluster have been estimated by several different methods to (m-M) in the range from 9.4 to 9.5, (Loktin & Beshenov 2001; Kharchenko, Pakulyak & Piskunov, 2003; Yakut *et al.*, 2003). Although the age have been determined by several groups to $\sim$ 20Myr, (18 $\pm$ 4Myr, Conti & Heuvel, 1970; 19Myr, Loktin & Besenov, 2000), we decided to use the age 28 Myr. For several clusters the age determined by Lithium dating have been about 50% higher than that found by fitting isochrones to the upper main sequence, (Basri 2000). The lithium dating is more robust since the turnoff age depends on the ammount of overshoot used. We decided to correct for this in our age.

1.3 Evolutionary models

Several groups have produced pre main sequence evolutionary models for low mass stars and BD's. Among these are the models by Girardi, *et al.*, (2000 & 2002), Baraffe, *et al.*, (1998, 2002 & 2003) and D'Antona & Mazzitelli, (1997). In this analysis we use the models by Baraffe, *et al.* They have produced three sets of models, BCAH98 (1998), DUSTY (2002) and COND (2003). Models without any form of dust which are valid at T$_{eff} \gtrsim$ 2300K (BCAH98). At lower temperatures dust start to form in the atmospheres and this needs to be taken into account. Models including the formation of dust and dust in the radiative transfer are valid at 2300K $\gtrsim$ T$_{eff} \gtrsim$ 1600K (DUSTY). For even colder BD's and planets the dust will settle gravitationally and should therefore not be included in the radiative transfer, dust formation should however be included. Such models should be used for $T_{eff} \lesssim 1300$K (COND). In the present analysis the BCAH98 models will most likely be sufficient. The faintest detections are at the boarder between the BCAH98 and DUSTY limits.

2 Observations

The two fields mentioned in section 1.2 observed by Michael Andersen in 1992 will in the following be named Field 1 and 2. When planning our observations we took into consideration the possibility to use these old data in combination with our own.

The observational prerequisites for this project were two half-nights with the optical instrument ALFOSC and one half-night with the NIR instrument NOTCam at the Nordic Optical Telescope, NOT. To detect brown dwarfs in the NCG 7160 cluster it was planned to observe it in the broad ALFOSC bands V and i. This primarily because the emission peak of brown dwarfs is in the IR (there is thus no use observing in the shorter wavelength bands), secondly the (V-i) color index is the temperature estimate most commonly used in optical color-magnitude diagrams (CMD's). In addition, the data may be combined with those from -92, although the extent of this project does not allow for that to be presented here. In NIR the cluster would be observed in K. The (i-K) color index is a sensitive temperature estimate, therefore are CMD's and color-clour diagrams (CCD's) based on this, tools to distinguish a set of probable cluster members and BD candidates.

To be able to relate the limiting magnitudes, received from S/N calculations, to masses (and temperatures) of observed objects we needed to use a model reaching down to the sub-stellar masses of brown dwarfs. We used the BHAC98 model, see Sec. 1.3, with a cluster age of 28 Myr to get the magnitudes shown in table 5. From the effective temperatures we estimated the spectral types listed in the first column.

The exposure times were derived from a signal-to-noise calculation program written by Michael Andersen. The basic assumptions were a telescope/system efficiency of 30%, a seeing of 0.8", a read-out-noise of 6 and a required S/N of 5. The resulting exposure times shown in table 5 might be a bit optimistic, but nevertheless show that we could go below the brown dwarf limit in an hour of exposure time, in all bands. The telescope time dedicated to the project would not be enough to go this deep covering the whole cluster. We instead decided to go deep in Field 1 and 2, imaged in 1992, and cover the whole cluster with a mosaic of shorter exposures. The first part would provide two methods to distinguish cluster members: Proper motions and color magnitude diagrams from the photometry. Additionally it should be possible to identify some brown dwarf candidates to maybe follow up with the lithium test. The second part would provide photometry-based membership of the brighter stars, a good estimate of the cluster size and possibility to model a complete mass function, MF, for the cluster.

2.1 Optical

The observation time dedicated to the project with the optical instrument ALFOSC at the NOT was 3.5 hours dark time (from 01.15 to 05.15 UT) for two nights, 7 hours in total. The wish was to go equally low (in mass) in both V- and i-band, regardless of the total exposure time. According to the BCAH98 model, the required exposure times increases very rapidly for masses below the brown dwarf limit, and there is no constant ratio between the exposure times of the two bands. To keep things simple, the decision was to have the total exposure time in the V-band double to that in the i-band, through the observations. In order to get the same quality of data in both fields, as is the case for the -92 data, we decided to observe both fields for the same amount of time, both nights. Of the 7 hours observing time with ALFOSC, 5 were dedicated to deep imaging, the remaining 2 for the mosaic and standards.

The read out from the CCD of ALFOSC may be performed in two different ways, the high or low gain mode. The high gain mode is most commonly used, because when observing objects of similar brightness, this shortens the exposure times and gives the lowest noise. But since our main interest was to get a large dynamical range, covering bright stars down to brown dwarfs, we chose the low gain mode. This also gave us the advantage of a shorter overhead time (OH) since the readout of the CCD is faster in this mode.

Since Field 1 and 2 were chosen to avoid the bright stars in the center of the cluster, we planned for 300 s exposures in both the V- and i-band. Including the OH, that mean that we had time for about 10 exposures per hour during the five hours dedicated to deep imaging. With 16 exposures per field in the V-band, half of that in the i-band, divided equal between the two nights, the total exposure time per night and field would be 40 minutes in V and 20 min in I. Investigating table 5, already one night's observations would reach down to about 50 M_J in both bands.

The field of view of ALFOSC is 6.5'×6.5'. The intention of the mosaic was to make 2×2 fields with 30" overlap, covering 12.5'×12.5' around the cluster center. These four fields (Fields a, b, c and d) contains both the very bright stars in the center of the cluster and fainter ones in the outskirts. It was decided to make 30 s exposures to get the fainter ones, letting the bright ones saturate, and instead complement with 3 s exposures of the central cluster, Field x. Four exposures of each of these five fields, in both bands, would take about 33 minutes, OH included. This plan should give us enough time left for observations of standard stars.

To observe standard stars the Landolt standard field SA92 (Landolt, 1992) was chosen, the coordinates are shown in table 4. The visibility plot of the targets (figure 1) shows that the best time to observe this field, with respect to airmass, was in the late night before twilight. To observe these standards were therefore in line with our main observing plans.

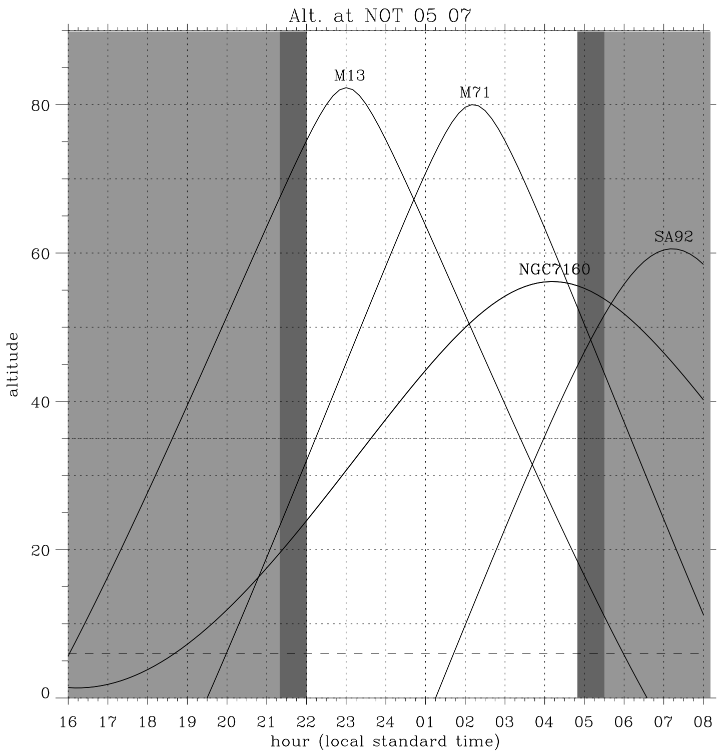

Figure 1: The visibility plot for the optical observations. SA92 is a Landolt standard field, while M71 and M13 are standard clusters for Stromgren photometry. Note that the observing run started at 01.15 LST.

Observations of the kind planned requires reasonably good seeing, or else the faint sources becomes too smeared out to be detected against the background noise. In the case of bad seeing ($\gtrsim$1.5") we were in need of a plan B. The Stromgren magnitude system consists of four bands, u, v, b and y, that are narrow compared to the UBV system, not overlapping. This makes the colors and effective temperatures obtained by these magnitudes more precise. Stromgren photometry of the cluster would thus give a well defined isochrone in a color-magnitude diagram, and it would be possible to derive its distance modulus. Including some Hβ narrow (Hβ_n) and wide (Hβ_w) observations would allow for another derivation of effective temperatures for F-type stars, through the ratio Hβ_n/Hβ_w. While this measure is not sensitive to dust extinction, as the temperatures from Stromgren photometry are, the combination of measurements would give an estimate of the dust extinction toward the cluster. Observing in these bands does not require good seeing, rather the opposite, since the stars we are interested in are bright and we do not want them to saturate the CCD. Therefore Stromgren u, b, v and y, plus Hβ_n and Hβ_w, imaging of the whole cluster made a good observing alternative in case of bad seeing. According to the visibility plot (figure 1) the M71 standard cluster (for Stromgren photometry calibration) was found at the approximately same airmass as NGC 7160 at the end of the night, while the M13 standard cluster had an appropriate elevation at the beginning of our observing run. This made them usable standards in case of bad seeing.

2.1.1 July 5 2003

The seeing during the night varied between 0".8 and 1".2 and it was possible to execute the primary observing plan.

Field 1 and 2 were imaged with 90° rotation between each exposure in the i#12 filter of ALFOSC, and with an additional offset of 5" for every other V filter exposure. Deep imaging went so smoothly, that the first fourth of the exposures planned for the second night was conducted as well. These were offset 5" in another direction relative to the first set of exposures. The total acquired exposure time per field was 25 minutes i-band and 50 minutes V-band.

Field a, b, c, d, x and SA92 were imaged twice in each filter with 90° rotation in between. We found that a mistake had been made when calculating the mosaic coordinates, causing the fields a, b, c, and d not to overlap in the intended way. There was no time to correct for this in the source catalog so the observations were carried out using these fields (see figure 2).

At twilight three flat fields were obtained in each filter as well as 10 darks.

2.1.2 July 7 2003

The seeing during the night varied between 1".0 and 2".2. This made it fruitless to go on with the broad band imaging, and plan B was instead realized.

Field 1 and 2 were each imaged once in the i-band and twice in the V-band (with 5" offset) before the decision was made to switch to Stromgren photometry. Field a, b, c, d and x were each imaged twice in y (30 s), b (40 s), v (60 s), y (120 s), Hβ_w (40 s) and Hβ_n (100 s) (single exposure times given in the brackets), with field rotation of 90° and -90° respectively. Field x was also imaged at field rotations 0° and 180° with these exposures, plus

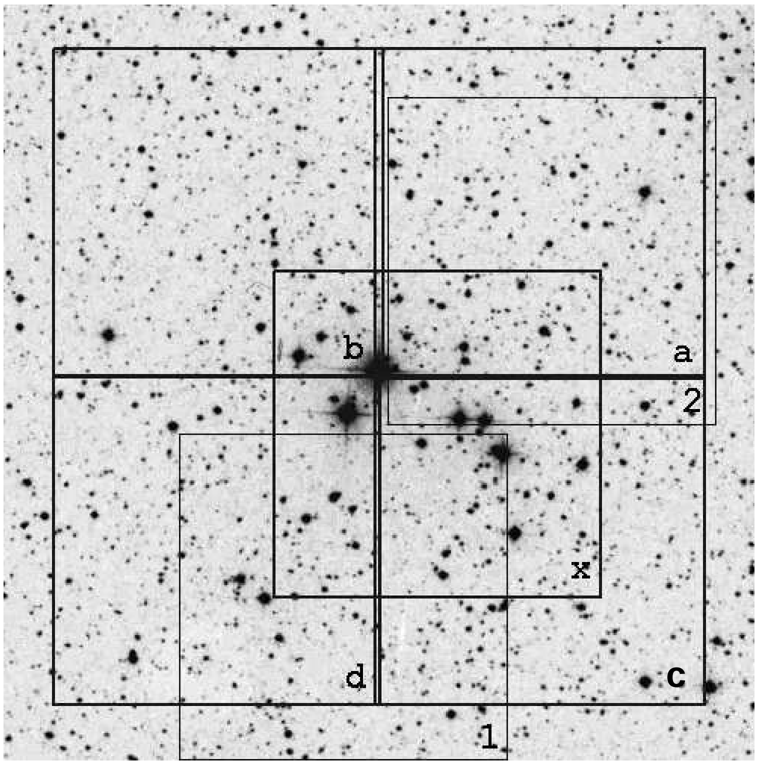

Figure 2: Illustration of the ALFOSC field positions in the cluster (field size 6.5'×6.5'). The optical image (E-band) is from the Digitized Sky Survey (DSS).

all four rotations using only 1/10 of the exposure time for each filter. Low gain mode was used for all the imaging.

M13 was imaged once in each filter in the beginning of the observing run, M71 at the end of the dark time. At twilight, six flat fields were obtained in each Stromgren filter, four flats in V and I respectively, and 20 darks.

2.2 Infrared

The near-IR instrument at NOT, the NOTCam, is equipped with three different K-band filters. The K_S-filter is the narrowest one, and also best centered between surrounding atmospheric absorption bands. 3.5 hours observing time (from 01.15 to 05.15 UT) with the NOTCam was dedicated to the project and it was decided to spend all that time imaging in the K_S-band. This should include both deep imaging of Field 1 and 2 and a mosaic, as in the optical. With the assistance of Anlaug Amanda Kaas, the exposure time required to reach a limiting magnitude of K_S=19 was estimated to be one hour for a wanted S/N of 5. According to the BCAH98 model (table 5) we would then reach object masses of the same order as those we reached in the i-band. The decision was made to prioritize the deep imaging and expose both fields for one hour. The remaining observing time should be planned carefully to obtain a mosaic.

The wide field of the NOTCam is 4'×4', smaller than both the fields of the -92 images and the acquired ALFOSC images. The central coordinates for the NOTCam deep imaging, given by Field 1_K and 2_K in table 4, were chosen to make them overlap completely with Field 1 and 2 while avoiding the brightest stars. The NOTCam detector would be saturated anyway, both for the deep imaging and the mosaic. Because of memory effects in the detector, an extra read-out (dark 0) then has to be made after each exposure, adding an OH of 6 s.

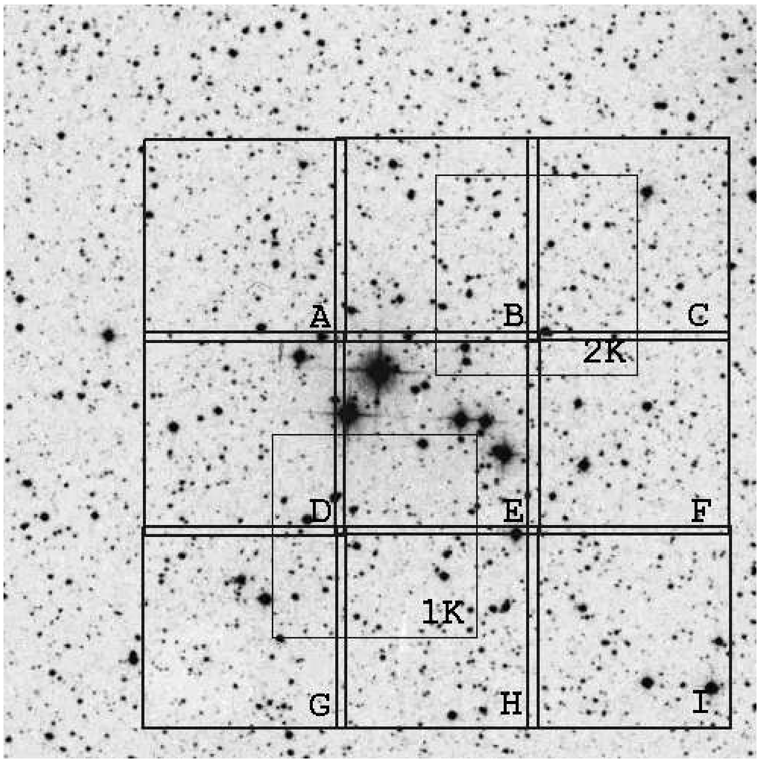

Figure 3: Illustration of the NOTCam field positions in the cluster (field size 4'×4'). The optical image (E-band) is from the Digitized Sky Survey (DSS).

It was decided to use the ramp-sampling mode for the readout of the NOTCam detector. The command line `>frame t N` then means that the voltage level over the detector should be read N times with t second intervals (non-destructive read-out). The linear regression of all the readouts then makes the resulting frame of t·N seconds exposure. Using `>frame 10 10` for the deep imaging would give 100 s exposure per frame. 5" dithering over nine positions was included in a script, giving 15 minutes exposure time and 18 minutes execution time (including OH) for the script. Thus, one hour exposure time for each of the two fields would in reality take 2 hours and 24 minutes, leaving a bit more than an hour for the mosaic and standards.

For the mosaic, 3×3 fields with 10" overlap would barely cover a 12'×12' area around the cluster center, approximately the same as in the optical mosaic. The `>frame 4 10` command would be good to use in these nine fields (Field A, B, C, D, E, F, G, H and I, see table 4 and figure 3), but the implementation needed to be as efficient as possible.

If including the dark readouts and telescope offsets between the fields in a script, the telescope does not move to its next position until the storing of the previous frame is completed. If instead a short script is used only for the frame and the dark, the telescope may be moved by a manual command to the TCS while the frame is stored. This would save us the storing time, 6 s, per frame exposed. For eight exposures per field, the short script decreases the execution time from 71 to 64 minutes, 7 minutes that could be well used for standards. In order to avoid unnecessary manual offsetting, a source catalog including both the set of nine fields and a corresponding set with the fields offset by 5" was created.

2.2.1 July 9 2003

The seeing during the night was about 1.0-1.2". Although the deep imaging had higher priority, the mosaic pattern observations were carried out first. This mainly because the chosen method, with a short script and manual offsets, required a high level of concentration from the operators/observers.

Field A-I were imaged eight times each, at four different field rotations and with a 5" offset between images of same rotation. Field 1_K and 2_K were imaged twice, using the nine positions dithering script of 900 s exposure each, at 90° relative field rotation. Then it was noticed that the exposure time was a bit too long, the sky background level reaching above the linear range of the detector. The script was modified to command `>frame 6 10` and tree more script runs were performed, at the remaining two field rotations and with an additional offset of about 4" for the last run. The total acquired exposure time per deep field ended up to be 57 minutes instead of one hour.

3 Reductions

In this section we concentrate on the different steps in the data reductions.

3.1 About CCD frames

Optical astronomical data mostly consist of data recorded by a CCD. A CCD image is a measurement of the digital output (the ADU, Analogue to Digital Unit) from every pixel in the CCD array. The main purpose of the initial reductions described in this section is to remove the effects added by the CCD itself.

The number of photons (N_p) that hit within a pixel will release a number of electrons (N_e) in the pixel. This process has the quantum efficiency $\mu(\lambda)$, that is; $N_e = N_p \cdot \mu(\lambda)$, where λ is the wavelength of the light. N_e is related to the output signal through an amplifier *gain* factor of unit "e^-/ADU", equivalent to "detected photons per ADU". If the CCD is linear the *gain* will be constant as a function of counts. During the amplification process a noise is introduced called the Read Out Noise (RON). This could result in negative analog outputs when the amount of counts is small. To avoid negative input at the A/D converter an electronic offset, significantly larger than the readout noise, is applied before the signal is converted to ADU. This offset is called the *bias*.

The digital output signal (S) from a pixel can now be written as:

$$S = \frac{N_p \cdot \mu(\lambda)}{gain} + bias + RON \tag{1}$$

All pixels in the CCD will have slightly different characteristics and there will be some pixel-to-pixel variations.

Apart from all effects introduced to the source signal from the CCD the light from an observed source will also have been distorted in a number of ways before it reaches the CCD. All these effects must be taken into account in the initial reductions in order for us to find the real source signal at each pixel (N_p). The following will describe how we performed these reductions.

3.2 Initial reductions

When reducing CCD images a number of standard initial reductions are applied to the data to correct for the CCD effects. Here we describe how we performed these reductions.

3.2.1 Bias and over-scan subtraction

First we subtract the *bias*. As explained the bias can be regarded as the signal coming from a pixel with no accumulated charge (that is 'no signal', or an empty pixel). The bias signal varies across the CCD such that there is more signal in pixels read out last. Furthermore there are also pixel-to-pixel variations in the bias. In this work we measure the bias structure by obtaining 40 bias frames. A bias frame is simply a readout of the CCD without opening the shutter or exposing. We simply computed the median of all the bias frames to obtain a master bias frame. This master bias frame was then subtracted from all the science and flat-field (see next section) frames.

3.2.2 Flat fielding

As mentioned the CCD sensitivity is not uniform across the whole of its surface. The response of the pixels can vary on all scales; from structures across the field to pixel-to-pixel variations. The variations of the response of the CCD, of the optics and of the instrument will all contribute to the sensitivity structure in the exposures. All these effects are mapped when obtaining a flat field image.

Flat field calibration frames are obtained by observing an evenly illuminated field using the same optical setup as that used to obtain object frames. We obtained these calibration frames as images of the twilight/dawn sky. We aimed for a high signal level (in the range 20-30000 counts/pixel) to reduce noise effects. From each flat field frame we subtracted the bias, and the flat-fields were then scaled and combined using the median. Then the combined flat-field was normalized. After the bias subtraction the science frames should be divided by the flat-field in order to take variations in the sensitivity of the system across the CCD into account.

3.2.3 Combining the science frames

After the initial reductions of the science frames the frames were combined to one. Between each exposure small offsets and 90 degrees rotation were applied in order to make systematic errors in the CCD and optics removable. Each frame will have different count levels (depending on the photometric conditions during the exposure) and different *seeing*. The seeing expresses the distortion of the light path on its way through the atmosphere and the telescope. It is measured as the Full Width Half Maximum (FWHM) of point sources in the field.

An IRAF procedure constructed by Michael Andersen ('*imreg*') was used to transform the science frames to a common coordinate system. These transformed frames could then be directly combined using the *imcombine* task in IRAF. The parameters in the imcombine was set as follows: The `combine` parameter was set to `average` but the `reject` parameter was set to `minmax` such that for each pixel position the pixel with maximal and minimal count level is rejected. The resulting pixel value is then the weighted average of the remaining pixels. The weight used here is the inverse square-root of the seeing in each frame. This was found to be the combination method that most effectively removed cosmics and CCD impurities and minimized the noise in the resulting frame.

3.3 Finding the signal from the source

After the initial reductions and the combination of frames the relative flux of objects across the field should correspond to the real relative flux of the objects.

Still, the flux in each pixel is a product of many things, and further reductions are needed to find the source flux. The signal in each pixel can be written as:

$$Counts(x, y) = C \cdot \langle S(x, y) \otimes PSF(x, y)\rangle \cdot t + SKY(x, y) \cdot t + RON \quad (2)$$

$S(x, y)$ is the signal from the source which will be convolved by the $PSF(x, y)$ Point Spread Function over the CCD. The PSF express the distortion of the light from the source through the atmosphere and telescope optics.

The task now is to find the real source signal $S(x, y)$ from each source in the field. We have done this by determining the PSF across the field and measure the observed flux of each source. Section 3.3.1 concentrates on the methods used to perform these reductions. In section 3.3.2 we explain how the calibration of the observed fluxes was performed.

3.3.1 Determining the PSF

As explained the Point Spread Function (PSF) is the distribution of light on the detector from a point-source outside the atmosphere. All stars can be considered to be point sources as can be seen from this simple argument. A typical star will have a radii (r) where $r \sim 10^{11}$m. But almost all stars have a distance from the earth (d) larger than 10^{17}m. By simple trigonometry the angular extension (ϕ) of a typical star will be: $\phi < 0.2''$.

After the initial reductions and the image combination one can model the PSF. All non-saturated stars in the field can be assumed to be point sources and hence used to determine the PSF in the field.

To do this can be difficult though. The PSF can depend on the position on the detector, the color and the brightness of the objects. We assumed that the PSF is constant across the field. We chose 10-20 suitable point sources (not to bright nor to weak and not to close to any other objects) across the field to compute the PSF. The software package DAOPHOT (Stetson 1997) was used to model the PSF. DAOPHOT fits an analytical function to the PSF, within a preselected fitting radius (set to 31pix for all frames). It subtracts the local sky value measured in an aperture of preselected radius (inner radius = 80pix, width = 11pix for all frames). It adds the fitted analytical function to a interpolated value derived from a table of residuals covering an area out to a preselected PSF radius. The analytical function used for fitting the PSF profile in this work is called `moffat25`.

After determining the PSF a PSF cleaning procedure was performed in order to improve the fitted PSF. We used the procedure `psfclean` programmed by Michael Andersen to do this.

3.3.2 Photometry

In order to calibrate the optical observations we observed the field of M71 and M13 as standard clusters for the Stromgren photometry. The Landolt (Landolt 1992) standard field SA92 was used to calibrate the broad band data. Initially, the calibration both in optical and in the infrared was done simply by fitting the zero-point m_0 in:

$$m = m_{DAOPHOT} + m_0 \tag{3}$$

For the optical data this zero-point was found by averaging the difference between the magnitude of the standard stars and the magnitude output of the DAOPHOT routine. As an example we show how the calibrations of the V band was performed:

First the standard magnitudes of the SA92 field stars were found (shown on table 1) In the calibration frames of the field these magnitudes are measured as well using aperture photometry with an aperture radius of 20 pixels. The measurements for V is shown on table 2. These measurements gave an average difference of $V_{std} - V_{aper} = -.1995 \pm 0.0465$. Now find the difference between the aperture photometry and the photometry used in DAOPHOT simply by using aperture photometry on a number of selected non-saturated stars. We get: $V_{aper} - V_{DAOPHOT} = 5.3000 \pm 0.0072$. This finally gives us a relation between the DAOPHOT output from our combined fields and the real magnitude of the object:

Table 1: Table of the standard magnitudes of the stars in the SA92 field.

standard	V(Landolt)
SA 92-245	13.8180±0.0028
SA 92-248	15.3460±0.0255
SA 92-249	14.3250±0.0049
SA 92-250	13.1780±0.0022

Table 2: Table of measured magnitudes.

standard	mg050205.imh	mg050207.imh
SA 92-245	13.688	13.614
SA 92-248	15.121	15.175
SA 92-249	14.064	14.120
SA 92-250	12.928	13.028

$$\begin{aligned} V &= V_{DAOPHOT} + 5.3000 \pm 0.0072 + 0.1995 \pm 0.0465 \\ &= V_{DAOPHOT} + 5.500 \pm 0.047 \end{aligned} \tag{4}$$

In the same way we also obtained the relation:

$$i = i_{DAOPHOT} + 5.019 \pm 0.039 \tag{5}$$

The infrared data was a bit more tricky to calibrate since we unfortunately typed in the wrong coordinates for the infrared standard star we did not have any standard star to perform the calibration. We therefore decided to use the 2MASS data for calibration of our data. We got:

$$K_s = K_{s,DAOPHOT} + 1.375 \pm 0.073 \tag{6}$$

Note that we in these reductions do not correct for reddening as we considered this not to be significant. According to Finkbeiner *et al.* (2000) the extinction factor would only be $A_V \sim 0.05$.

Unfortunately, when constructing a color color diagram of the cluster the sequence of stars did not follow the isochrone (of age 28Myr) but was offset from this. We interpreted this as an offset in the zero-point computed above and we fitted new zero-point for our data such that the condensed sequence

Table 3: Magnitude zero-points (zp) for the different filters in field 1 and 2, such that $m_{i,V,K_s}(res) = m_{i,V,K_s}(DAOPHOT) + zp$.

Filter	Field 1	Field 2
V	4.8	5.4
i	4.7	5.2
K_s	1.95	1.95

of stars in the color-color diagram are exactly on the isochrone in the high-mass end. This turned out to be different offsets for the different fields. We found the zero-points displayed on table 3.

Besides the zero-points we also included color terms for the i band, such that $i = i(res) + 0.055(i(res) - K_s(res))$, where $i(res), K_s(res)$ are the magnitudes found when adding the zero-points given in table 3 to the DAOPHOT magnitude outputs.

Now with this presumably better calibration of our data we have the problem of understanding why we get different zero-point for the different fields. Since these fields are observed using exactly the same setup we had expected the offsets to be of similar size. The offsets are: $V_{field1} - V_{field2} = -0.6$, $i_{field1} - i_{field2} = -0.5$ and no offset in K_s.

In spite of these unexplained offsets we have chosen to use the zero-points found by fitting to the models (and displayed in table 3) in our further analysis.

4 Results

4.1 Diagrams

Before any diagram can be done, the stars found from the smaller NOTCam field have to be identified from larger ALFOSC field. This was done using IDL procedure `trfm_coords.pro` by Michael Andersen. This procedure fits a linear coordinate transformation of a set of input coordinates (X,Y) onto a set of reference coordinates (X0,Y0), and then applies affine transformation to a set of input data. This procedure is not however totally straight forward because during the transformation from K_S-band coordinates into i-band coordinates there are quite large residuals, which probably mean that there are (non-linear?) distortions between two images, i.e. the two instruments distort differently. But the more reference stars are used the better and they should be scattered over as large part of the smaller field as possible. In this case, 8 reference stars were used per field.

When the coordinates of the optical and IR fields are finally more or less the same, we can try to find stars which are in both fields. This is done using IDL procedure `ik_match.pro` by Michael Andersen. In this procedure a routine which matches 2 or 3 sets of 2D float data points is used – in our case 2 and 3 coordinate lists, i-band with K_S-band, and i-band with V-band and K_S-band. The simple linear transformation is not the sufficient one, but using tolerance of 2 pixels in matches, between i-band and K_S-band there were about 900 matches, and between i,V and K_S-bands there were about 800 matches.

4.1.1 Color-magnitude diagram

To identify possible brown dwarf candidates from the cluster, we made a color-magnitude diagram with BCAH98 model which has been corrected to apply distance modulus of 9.40 (Loktin & Beshenov 2001; Kharchenko, Pakulyak & Piskunov, 2003; Yakut *et al.*, 2003).

Candidates are the stars which are on right hand side of the plotted BCAH98 model in this (i-K_S),i -diagram, i.e. they are mostly red and faint but in some cases they are also solar type stars, and have mass less than $\sim 0.070 M_\odot$.

The final color-magnitude diagram, where is used stars from both fields, is shown in Fig. 4. As can be seen, there are some good BD candidates in the cluster, indeed.

In Fig. 5 is shown 'pseudo differential distance modulus', i.e. i-magnitude difference, of all the stars in color-magnitude diagram relative to a 28 Myr

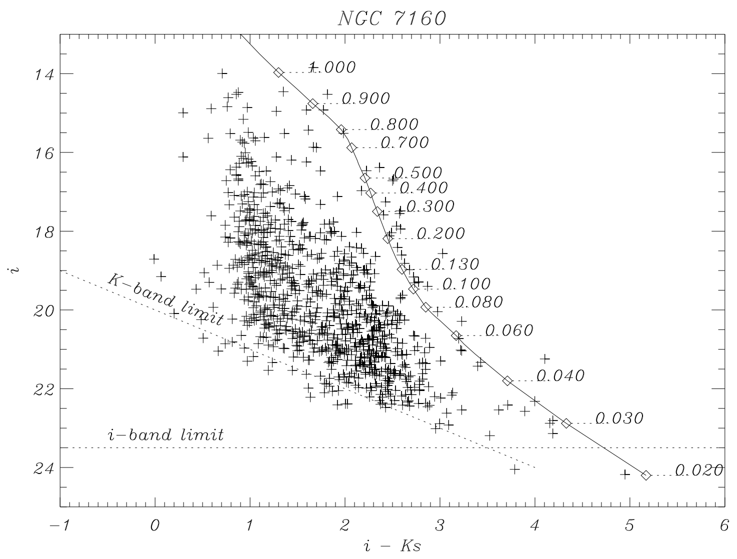

Figure 4: Color-magnitude diagram for NGC 7160. The isochrone comes from BCAH98 model.

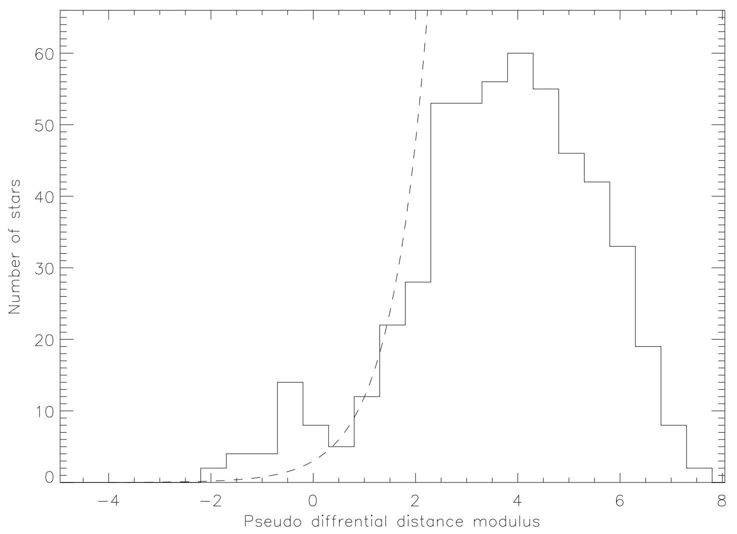

Figure 5: Pseudo differential distance modulus, i.e. i-magnitude difference, of all the stars in color-magnitude diagram relative to the model isochrone. Cluster is very likely at left most small spikes in histogram.

model isochrone. The figure shows that most of the stars are 4 – 6 mags from the model, but the small spikes at left part of the histogram are very likely from the cluster.

4.1.2 Color-color diagram

From our data we can build up a color-color diagram using (V-i):(i-K_S) and find out information about temperatures and metallicities [m/H] as done by Leggett et al. (1998) using NextGen models (Allard et al. 1997; Hauschildt et al. 1999).

The final color-color diagram, where is used stars from both fields, is shown in Fig. 6. Into the figure is also plotted an isochrone using BCAH98 model.

When this color-color diagram is compared with corresponding diagram by Leggett et al. (1998), it roughly seems that stars more massive than $\sim$0.95$M_\odot$ have T_{eff}=4000K, the stars more massive than $\sim$0.80$M_\odot$ have T_{eff}=3500K and the stars more massive than $\sim$0.08$M_\odot$ have T_{eff}=3000K. The model isochrone follows quite nicely NextGen model sequence for metallicity [m/H]=0.

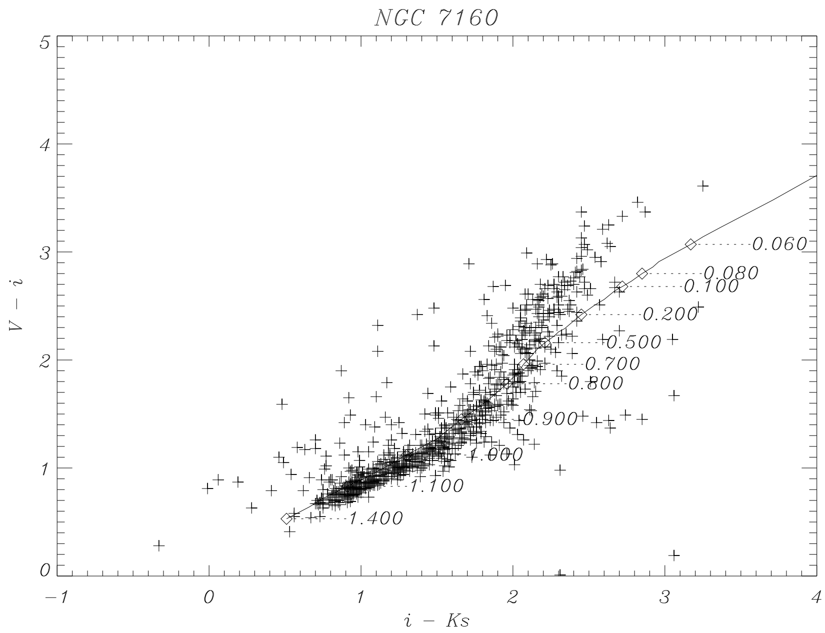

Figure 6: Color-color diagram for NGC 7160. The isochrone comes from BCAH98 model.

4.2 Brown dwarf candidates

In Fig. 7 we have a closer look into color-magnitude diagram shown in Fig. 4. However, now only the stars around interesting region are plotted. From this figure can be selected 20 candidates. Stars are chosen using criteria mentioned in Sec. 4.1.1, but since there are some errors in magnitudes, also some stars from other side of the isochrone are chosen. 11 of these stars are in field 1 and 9 of them are in field 2.

Next thing was to identify these candidates and mark them into NOTCam K_S-band fields (Fig. 8 and Fig. 9). Candidates are marked using pink circles and candidate is always the star just in the middle of the circle. At least one identification has to be wrong, since it's in very edge of the IR field 1. Also, some of the candidates were very clearly seen in i-band images, but in K_S images they were just barely seen.

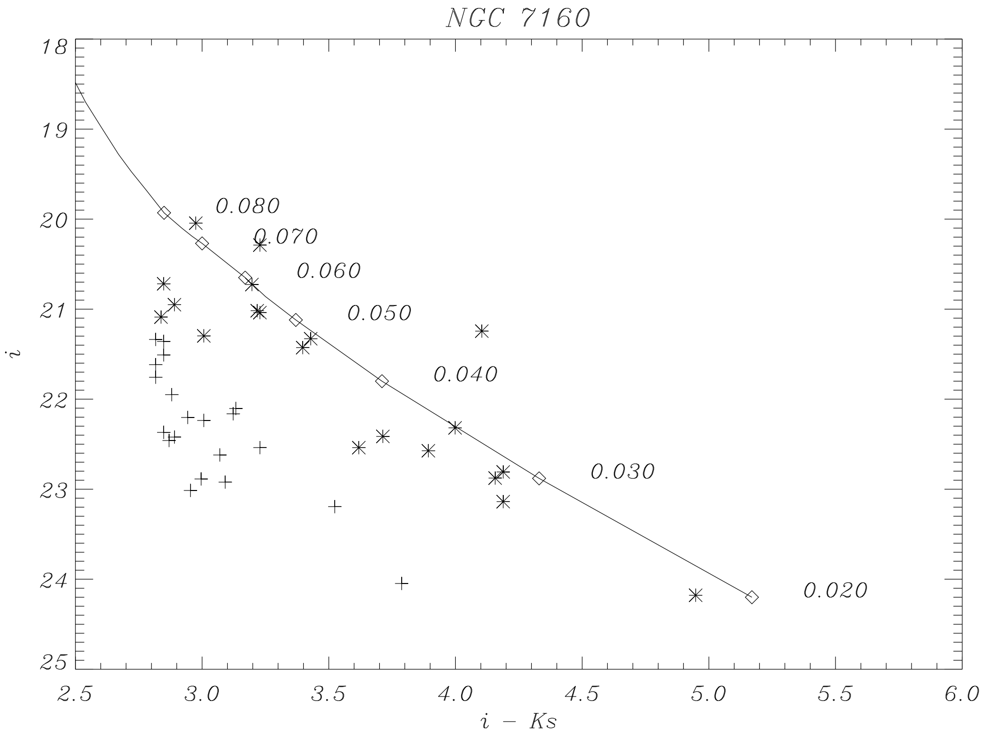

Figure 7: Closer look into color-magnitude diagram. Only stars around interesting part of the diagram are plotted. Candidates are plotted using *-symbol.

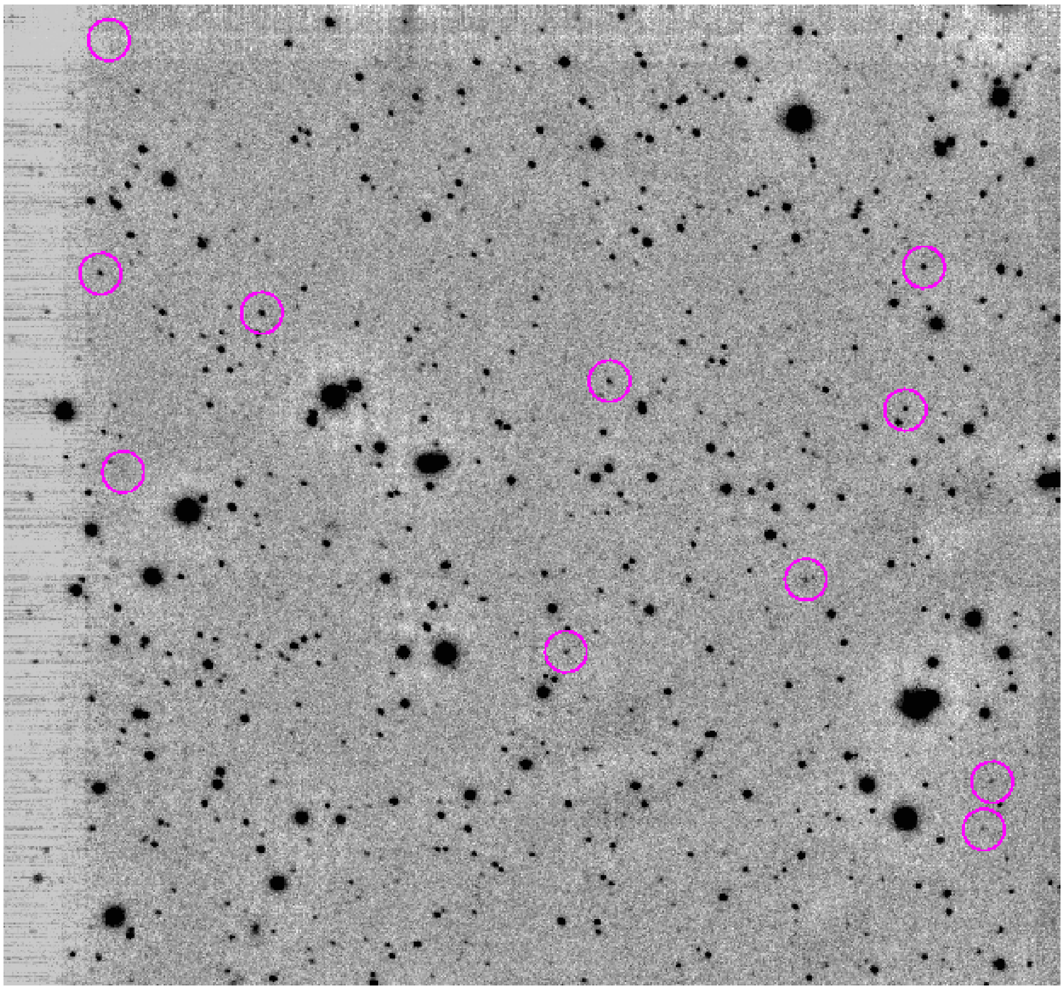

Figure 8: BD candidates marked with pink circles into NOTCam field 1 (see Fig. 3 for position of the field in cluster).

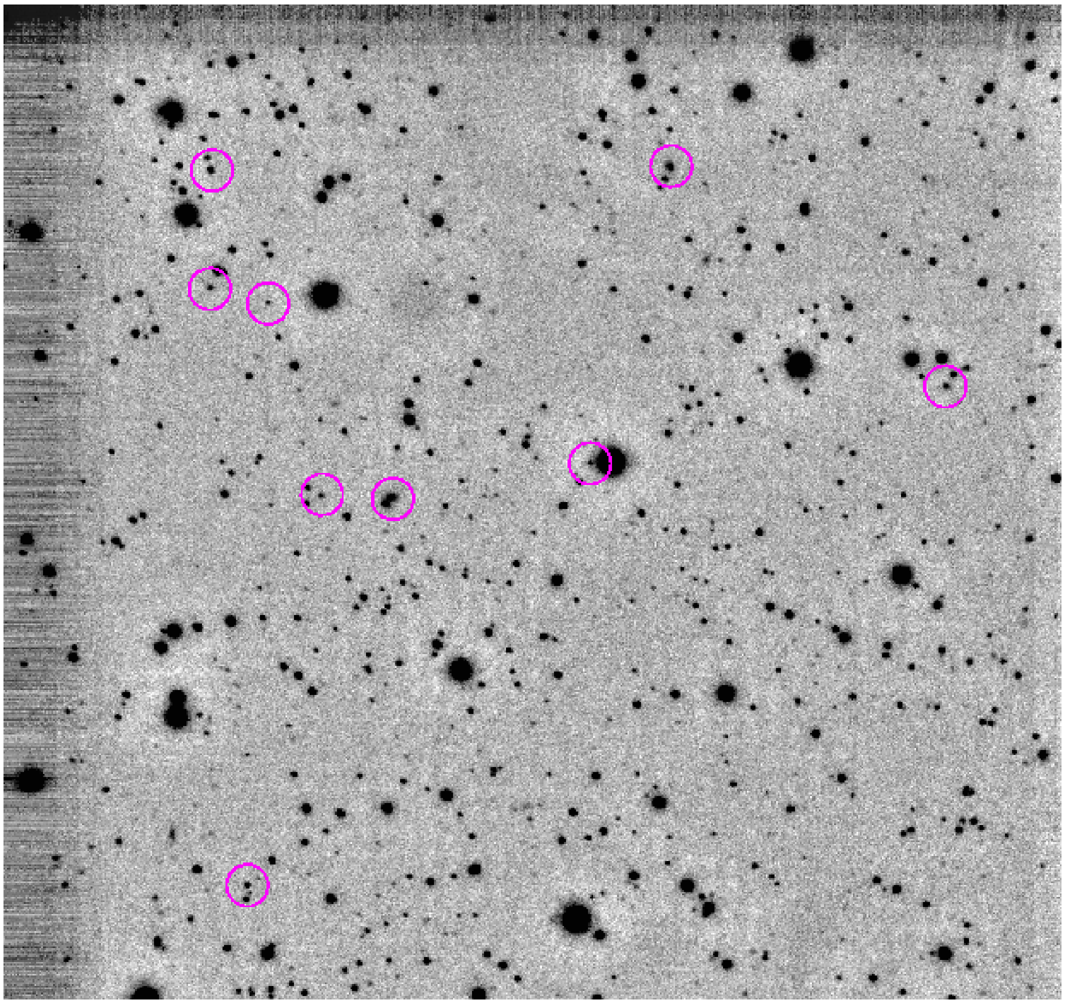

Figure 9: BD candidates marked with pink circles into NOTCam field 2 (see Fig. 3 for position of the field in cluster).

4.3 IR-mosaic

The mosaics of the cluster (Fig. 10) were made to get a overall picture of the cluster and maybe in later point a true color image will be done.

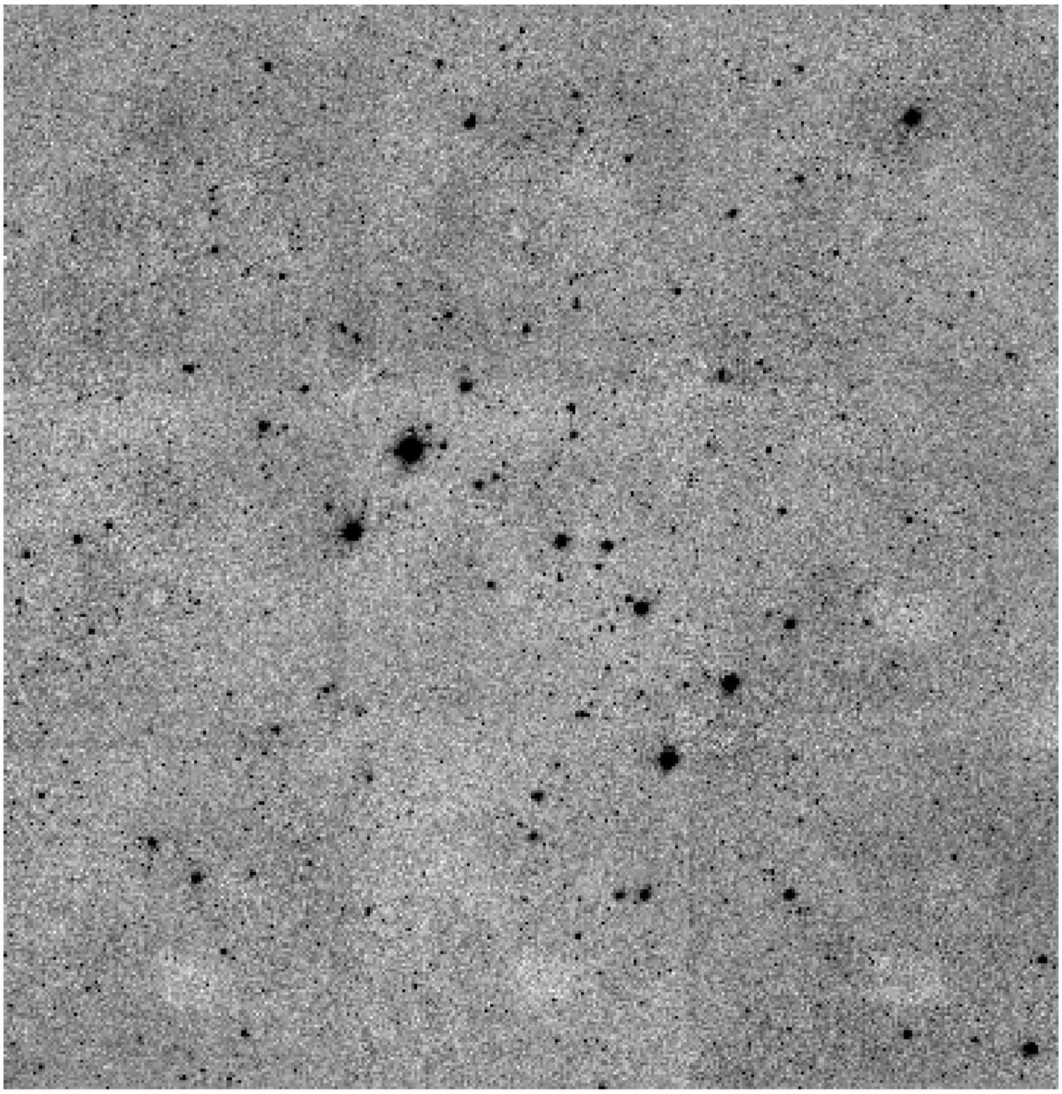

Figure 10: Mosaic of the cluster made using 9 4'x4' NOTCam K_S-band images with 10" overlap. In the image N is up and E is to left.

5 Future work

5.1 New diagrams

We have observed more V-band and i-band data during 2nd of August in order to go deeper in optical. This data has to be also reduced and combined with the summer school data.

5.2 Mosaics of the cluster

As already mentioned in Sec. 2, both in optical and in IR we have observed a mosaic of the cluster – in optical using 4 smaller boxes and in IR using 9 boxes. Combining these individual images we can get an overview of the hole cluster and combining images in different bands we can get a true color image of the cluster, and maybe some kind of idea about the size of the cluster.

5.3 Mass function

From color-magnitude diagram we can select probable or possible cluster members and use these stars to derive mass function of the stellar population of the cluster, and compare its slope to the value measured for the Pleiades ($\alpha = 0.75$) and Alpha Persei ($\alpha = 0.59 \pm 0.05$).

5.4 Proper motions

Since we have older photometric data from the same fields taken in 1992, we will also be able to derive proper motions to establish cluster membership. The proper motion of the cluster suggested in literature are of the order 3 to 4 mas/yr (Rastorguev *et al.* 1999; Kharchenko, Pakulyak & Piskunov 2003; Yakut *et al.* 2003).

5.5 MOS plates

With Multi Object Spectroscopy (MOS) we can study spectra of the BD candidates and get this way a confirmation which candidates really are BD's and which are something else. If object show to have lithium in their spectrum, it is definitely a BD. The lithium test works down to the minimum main sequence temperature, below which all objects are automatically BD's (Basri 2000). However, at the age of NGC 7160 also LMS will show lithium because it has not been depleted. All the stars, which show lithium, are definitely members of the cluster, if not BD's.

5.6 Light curve inversions

The very young BD's seem to show strong magnetic activity (Neuhäuser & Comeron 1999). These are sufficiently luminous objects that are hot enough and/or perhaps not rotating too fast. In the youngest cases, there may be an added contribution due to accretion phenomena. However, all of these become eventually relatively inactive as the convection weakens and the atmosphere cools. Most objects near or below sub-stellar boundary are apparently rapid rotators because they have not experienced much magnetic breaking. (Basri 2000)

In this young cluster, the stars are supposed to be very active and rapidly rotating, which means that they are likely to have cool spots on their surfaces. From photometric light curves (Johnson V-band) of the stars in the field, we can select the ones, which show brightness variations in their light curves, and consider them as members of the clusters.

Later, the light curves of chosen stars can be inverted into stellar images using approach developed by Berdyugina et al. (2002), which is based on the Occamian inversion technique (Berdyugina 1998).

Acknowledgment

This is a report from the NORFA research course on observational astrophysics at the Nordic Optical Telescope (the NOT) at La Palma July 1-12 2003. The data presented in this report was obtained using the NOT.

This publication also makes use of plates from the Digitized Sky Survey, produced at the Space Telescope Science Institute under U.S. Government grant NAG W-2166. The images of these surveys are based on photographic data obtained using the Oschin Schmidt Telescope on Palomar Mountain and the UK Schmidt Telescope.

Finally, this publication makes use of data products from the Two Micron All Sky Survey, which is a joint project of the University of Massachusetts and the Infrared Processing and Analysis Center/California Institute of Technology, funded by the National Aeronautics and Space Administration and the National Science Foundation.

Appendix A

We here show the tables referred to in section 2.

Table 4: Positions of observed fields (J2000 coordinates).

Field	Ra (h m s)	Dec ($\circ$ $'$ $''$)
ALFOSC fields:		
Field 1	21 53 54	62 32 23
Field 2	21 53 18	62 39 02
Field a	21 53 20	62 40 00
Field b	21 54 16	62 40 00
Field c	21 53 20	62 33 30
Field d	21 54 16	62 33 30
Field x	21 53 38	62 35 38
SA92	00 54 27	00 40 00
M71	19 53 41	18 48 42
M13	16 41 41.5	36 29 37
NOTCam fields:		
Field 1_K	21 53 49	62 33 37
Field 2_K	21 53 21	62 38 48
Field A	21 54 11	62 39 28
Field B	21 53 38	62 39 28
Field C	21 53 05	62 39 28
Field D	21 54 11	62 35 38
Field E	21 53 38	62 35 38
Field F	21 53 05	62 35 38
Field G	21 54 11	62 31 48
Field H	21 53 38	62 31 48
Field I	21 53 05	62 31 48

Table 5: Results of the BHAC98 model and S/N calculations.

SC	Mass [$M_\odot$]	Age [Myr]	T_{eff} [K]	L_{Bol}	V	I	K	t_{exp}V [s]	t_{exp}I [s]	t_{exp}K [s]
M7	0.020	28.3	2156	-3.300	29.57	24.80	19.63	-	3300	
M7	0.030	28.6	2431	-3.060	27.45	23.48	19.15	50000	300	3600
M6	0.040	28.4	2639	-2.830	25.88	22.40	18.69	2500	50	
M5	0.050	28.4	2768	-2.670	24.95	21.72	18.35	500	19	
M5	0.055	28.4	2816	-2.600	24.60	21.46	18.21	280	14	
M5	0.060	28.5	2856	-2.550	24.32	21.25	18.08	180	11	
M4	0.070	28.4	2930	-2.450	23.81	20.87	17.87	85	7	
M4	0.072	28.3	2948	-2.430	23.70	20.79	17.83	72	6	
M4	0.075	28.6	2970	-2.400	23.56	20.70	17.78	60	6	
M4	0.080	28.6	3005	-2.350	23.33	20.53	17.68	45	5	
M4	0.090	28.3	3049	-2.270	23.01	20.28	17.50	30	4	
M3	0.100	28.3	3087	-2.210	22.75	20.07	17.35	23	3	
M3	0.110	28.3	3118	-2.140	22.52	19.88	17.21	18	2	
M3	0.130	28.5	3173	-2.040	22.13	19.57	16.97	12	2	
M3	0.150	28.4	3219	-1.950	21.81	19.30	16.76	9	1	
M2	0.175	28.4	3261	-1.850	21.49	19.03	16.54	6	1	
M2	0.200	28.3	3298	-1.760	21.21	18.79	16.34	5	<1	
M2	0.250	28.4	3360	-1.630	20.76	18.41	16.02	3	<1	
M2	0.300	28.4	3414	-1.510	20.39	18.10	15.76	2	<1	
M2	0.350	28.5	3452	-1.420	20.11	17.85	15.55	2	<1	
M2	0.400	28.4	3489	-1.340	19.85	17.63	15.36	1	<1	
M1	0.450	28.4	3523	-1.270	19.63	17.44	15.20	1	<1	
M1	0.500	28.3	3561	-1.200	19.41	17.25	15.04	1	<1	
M1	0.570	28.2	3624	-1.110	19.09	16.99	14.83	<1	<1	
M1	0.600	28.4	3655	-1.070	18.95	16.88	14.74	<1	<1	
M0	0.620	28.6	3676	-1.040	18.86	16.81	14.68	<1	<1	
M0	0.700	28.2	3781	-0.920	18.44	16.48	14.41	<1	<1	
M0	0.750	28.2	3859	-0.840	18.15	16.27	14.24	<1	<1	
K9	0.800	28.3	3956	-0.750	17.80	16.02	14.06	<1	<1	
K8	0.850	28.4	4100	-0.650	17.33	15.71	13.88	<1	<1	
K7	0.900	28.3	4273	-0.530	16.81	15.36	13.70	<1	<1	
K5	0.950	28.3	4472	-0.390	16.27	15.00	13.50	<1	<1	
K2	1.000	28.3	4722	-0.230	15.69	14.57	13.27	<1	<1	
K0	1.050	28.2	5038	-0.050	15.06	14.10	13.00	<1	<1	
G8	1.100	28.4	5381	0.150	14.45	13.62	12.71	<1	<1	
G6	1.150	28.7	5681	0.220	14.22	13.48	12.70	<1	<1	
G2	1.200	28.5	5793	0.210	14.23	13.52	12.78	<1	<1	
G0	1.300	29.2	6019	0.340	13.87	13.23	12.57	<1	<1	
F5	1.400	28.2	6498	0.540	13.34	12.81	12.30	<1	<1	

Bibliography

Allard, F., Hauschildt, P.H., Alexander, D.R. & Starrfield, S. 1997, ARA&A, **35**, 137

Baraffe, I., Chabrier, G., Barman, T. S., Allard, F., & Hauschildt, P. H. 2003, A&A, **402**, 701

Baraffe, I., Chabrier, G., Allard, F., & Hauschildt, P. H. 2002, A&A, **382**, 563

Baraffe, I., Chabrier, G., Allard, F. & Hauschildt, P. H. 1998, A&A, **337**, 403

Basri 2000, ARA&A, **38**, 485

Berdyugina, S.V. 1998, A&A, **338**, 97

Berdyugina, S.V., Pelt, J. & Tuominen, I. 2002, A&A, **394**, 505

Finkbeiner, Davis & Schlegel, 2000ApJ,**544**, 81

Chabrier & Baraffe, 2000, ARA&A, **38**, 337

Conti, P. S. & van den Heuvel, E. P. J. 1970, A&A, **9**, 466

Cutri, *et al.*, 2003, yCat, 2246, 0

D'Antona & Mazzitelli, 1997, MmSAI **68** 807

Girardi, *et al.*, 2002, A&A **391** 195

Girardi, *et al.*, 2000, A&AS **141** 371

Hauschildt, P.H., Allard, F. & Baron, E. 1999, ApJ, **512**, 377

Kharchenko, Pakulyak & Piskunov, 2003, ARep, **47**, 263

Landolt, A. U. 1992, AJ, **104**, 340

Leggett, S.K., Allard, F. & Hauschildt, P.H. 1998, ApJ, **509**, 836

Loktin & Beshenov, 2001, AstL, **27**, 386

Neuhäuser, R. & Comeron, F. 1999, A&A, **350**, 612

Rastorguev, A.S., Glushkova, E.V., Dambis, A.K. & Zabolotskikh, M.V. 1999, AstL, **25**, 595

Stetson, 1997, "User's Manual for DAOPHOT II"

Williams, 1995, PhDT, 21

Yakut, *et al.*, 2003, A&A, **405**, 1087

2MASS survey: http://www.ipac.caltech.edu/2mass/releases/allsky/